

Design feasibility of gamma camera without collimator based on specific arrangement of the detectors

Hossein Akbari-Lalimi^{1,2} · Seyed Ali Shafiei³

Received: 28 October 2015 / Revised: 10 May 2016 / Accepted: 11 May 2016 / Published online: 11 July 2016
© Shanghai Institute of Applied Physics, Chinese Academy of Sciences, Chinese Nuclear Society, Science Press China and Springer Science+Business Media Singapore 2016

Abstract In gamma camera and single-photon emission computerized tomography, the collimator removes most photons. Here, a gamma camera without collimator utilizes a specific arrangement of detectors. Instead of bending beams (like a lens) or directing beams (by parallel hole collimator), changes are created in detectors' field of view (FOV), so that each detector's FOV looks different from others. Simulation proved this theory, with 98 detectors (2 cm × 1.41 cm) arranged in a zigzag manner for Monte Carlo simulation. A radioactive source with energy of 140 keV was situated on the detectors' faces. Sixty projections, each 3° (0°–179°) apart, were simulated by Monte Carlo N-Particle (MCNP) 4C code, rotating detectors around a radioactive point. The band containing the radioactive source is clearly visible in each projection. Counts obtained after simulation in different projections were reconstructed, and point source location emerged correctly. Simulation of gamma camera with zigzag arrangement of detectors and MCNP-4C code demonstrated that one could string the space and determine radioactive source by image reconstruction without using

collimators, solely through these special detectors' distribution.

Keywords Collimator · Gamma camera · SPECT · Monte Carlo simulation

1 Introduction

To be able to photograph an object, there should be a one-to-one correspondence between an object and its image. The lens performs this function in an ordinary photographic camera. However, a lens cannot create such a correspondence for high-energy radiation, since lenses ordinarily are not able to bend high-energy radiation [1]. Therefore, nuclear imaging (SPECT and gamma camera) is conducted with the help of a radioactive uses aperture (pinhole) and parallel hole collimator (PHC) to direct output radiation from the body. In this way, a one-to-one correspondence is created between radiopharmaceutical distribution in the body and its image [2].

Many studies [3–6] have been conducted in the effort to find appropriate methods for design and construction of collimators of gamma-ray imaging systems. Three such influential studies are the Jaszczak et al. [4] study assessing cone beam collimators; the Tsui et al. [5] research on the assessment of fan beam collimators; and that of Mueller et al. [6], which selected high-resolution low-energy collimators in brain imaging.

One type of collimator is the pinhole collimator (PC), which is comprised of a small pinhole aperture embedded in a piece of lead or tungsten. In PCs, where there is a small object next to the collimator aperture, there usually is good

This work was supported by grants from Rafsanjan University of Medical Sciences, Rafsanjan, Iran.

✉ Seyed Ali Shafiei
sashafiei@muq.ac.ir

¹ Geriatric Care Research Center, Rafsanjan University of Medical Sciences, Rafsanjan, Iran

² Department of Medical Physics, Mashhad University of Medical Sciences, Mashhad, Iran

³ Department of Physiology and Pharmacology, School of Medicine, Qom University of Medical Sciences, Qom, Iran

spatial resolution and detection efficiency, but the field of view (FOV) becomes smaller [7]. Such collimators are used in humans to image some body parts such as the wrist and thyroid [7, 8] and are only rarely used for heart and breast [9, 10]. The greater the distance between the object and the PC's aperture is, the greater the FOV is, and the less the spatial resolution and sensitivity is. On the other hand, the sensitivity will be increased by using a pinhole aperture of large diameter that leads to a decrease in resolution. The more the apertures focus on different points in the FOV, the larger the FOV. Additionally, the higher the sensitivity, the better the spatial resolution [11]. Many studies select the proper parameters to improve the above-mentioned quantities [12, 13]. However, using single aperture eliminates most photons containing information. The sensitivity, FOV, and spatial resolution will rise if apertures are increased [14–16].

Therefore, one of the methods employed to decrease the number of removed photons containing information is to use a thick lead plate with holes (PHC), in which all beams parallel to its holes are allowed to cross [2].

Designing the proper PHC depends on the application, sensitivity, and necessary resolution. Hence, it is constructed in different forms and designs, and the real performance of the best design will usually be assessed empirically [17, 18]. The major problem with PHCs remains the elimination of useful information-containing beams, i.e., of every 10,000 photons, just one is allowed to cross the collimator [19]. This leads to an increase in imaging time and patient-injected radiopharmaceutical dose, and a decrease in image quality.

Since the number of emitted photons is generally very low, collimators have the most important restrictions in gamma camera and SPECT. Consequently, a great step forward will be taken if a radiopharmaceutical spatial distribution in the body is obtained by using a gamma camera without a collimator.

The aim of this study was to present the idea of a gamma camera without collimator (GCWC) based on the specific arrangement of detectors in zigzag form. Ideally, this theory will be assessed through Monte Carlo simulation by MCNP code.

2 Materials and methods

2.1 Theory

In GCWC, instead of using a series of detectors on a flat plate together with a large crystal, gamma detectors are distributed in zigzag form to create a row of detectors (ROD) (Fig. 1). Detector rows are separated with lead plates, called septa.

In other words, instead of bending the beams (like a lens) or directing the beams (by collimators), some changes are created in the detectors' FOV in such a way that the FOV of each detector will be different from those of the other detectors (Fig. 2). In this way, the observation of radiopharmaceutical distribution in space will be unique for different detectors. The image can be produced by using the difference in observed radiopharmaceutical distribution and image reconstruction through the filtered back projection (FBP) method, without the necessity of a collimator.

GCWC is designed in such a manner that distribution of detectors is shaped in a zigzag manner. As a result, the FOV of each detector on the right side of each triangle in Fig. 2 is different from the adjacent detector by merely a strip (similarly, this is true for the detectors on the left side of the triangle). In other words, detectors D_1 and D_2 observe radioactive source S' , but only detector D_1 (out of the detectors on the right side) detects source S .

Therefore, if a radioactive material is laid in front of this detector distribution (each ROD), $N_{D_1} - N_{D_2}$ equals the absorbed radiation resulting from radioactive materials in the shaded bar (N_{D_1} and N_{D_2} are, respectively, the number of counts read by detectors D_1 and D_2). In other words, a narrow strip containing radioactive material will be separated without the necessity of eliminating beams through using hardware similar to a PHC.

The imaging is staged in two perpendicular projections; point S is shaped from the intersection of two bands through $(D_{0i} - D_{0i+1})$ and $(D_{90j} - D_{90j+1})$ (Fig. 3). Therefore, point S can be determined through image reconstruction by FBP. $D_{\varphi\alpha}$ indicates the α th detector in the projection angle of φ° .

Apparently the proposed idea can be implemented theoretically, but its accuracy and verification must be proven through simulation. Therefore, the following sections will investigate the feasibility of this idea, ideally through simulation based on Monte Carlo with MCNP code.

2.2 Computer simulation

Monte Carlo method is based on random sampling to find solutions for physics or math problems according to certain probabilities and laws of statistics. In addition, it is highly accurate in predicting the outcomes of processes that are repeated many times. Monte Carlo simulation (MCS) using MCNP code is a common method in gamma camera imaging and designing proper collimator experimentation [18, 20].

Ninety-eight detectors were arranged in a zigzag manner on a line 1 m in length, which formed a ROD for MCS. Dimensions of each detector's surface were 2 cm \times 1.41 cm. Therefore, the thickness of the imaging slice that was taken by

Fig. 1 GCWC in three dimensions: A, distance between two lead septa, detector width, and thickness of image slice; B, row of detectors (ROD); C, septa between detector rows

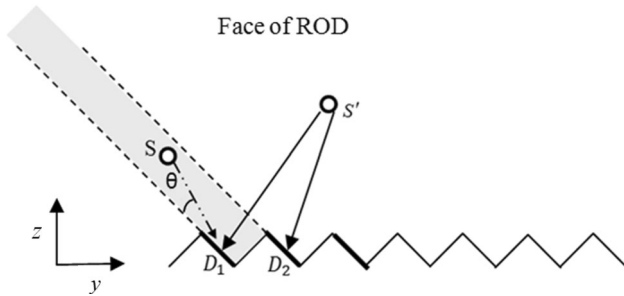
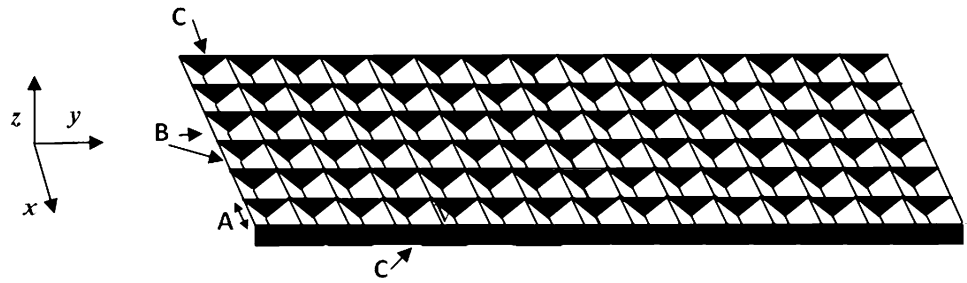


Fig. 2 One detector row: Shaded bar is the difference between two FOVs of detectors, so that radioactive source *S* is observed only by detector *D_j*; the face of ROD: the slice that ROD and some radioactive material laid on it; θ : angle between the incident radiation and detector level

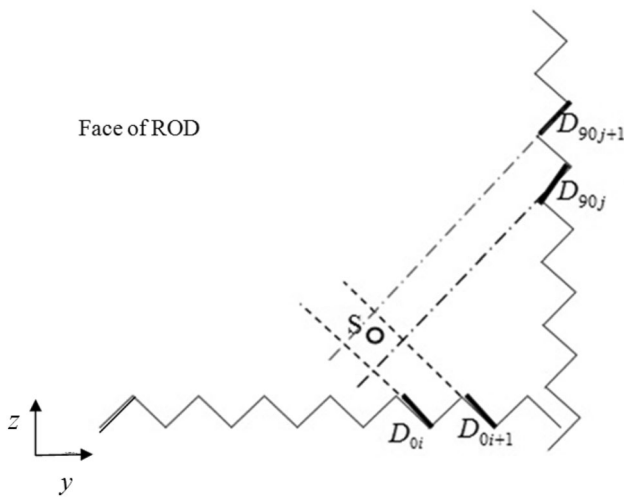


Fig. 3 Point *S* is shaped from the intersection of two bands through two perpendicular projections, $S \in (D_{0i} - D_{0i} + 1) \cap (D_{90j} - D_{90j} + 1)$, where *i* and *j* are number of detectors

ROD was 2 cm. Technetium-99m (which has an energy of 140 keV) radiopharmaceuticals are in widespread use for imaging and functional studies (over 80 % of all diagnostic procedures) of major organs such as the heart, brain, liver, kidney, and thyroid [21]. Therefore, a radioactive source with energy of 140 keV was situated on the face of the ROD, i.e., the slice on which the ROD and some radioactive materials

have been placed (Figs. 2 and 3). Among the active detectors, 49 detectors were laid on the right side of the triangle in ROD. Sixty projections at a distance of 3° (0° – 179°) from each other were simulated by MCNP-4C code. In other words, simulation was performed 60 separate times, with 60 different projections at a distance of 3° , and the photons passing through each detector were counted. It was verified that in each simulation period, 100,000,000 photons were released from the radioactive source and were traced by MCS.

3 Results

After simulation and data collection, each detector's counts were estimated in different projections. For example, Fig. 4 shows the first projection (angle of 0°) in which the vertical axis is the gamma-ray counts and the horizontal axis is the number of detectors on the right side of the zigzag arrangement.

In Fig. 2, the number of counts necessary for the relevant strip will greatly decrease with the angle between the incident radiation and detector surface. Therefore, Eq. (1) observes the number of counts resulting from the difference counts of two consecutive detectors. $D_{\varphi\alpha}$ indicates counts of the α th detector in the projection angle of φ° . Two consecutive detectors determine the bandwidth value

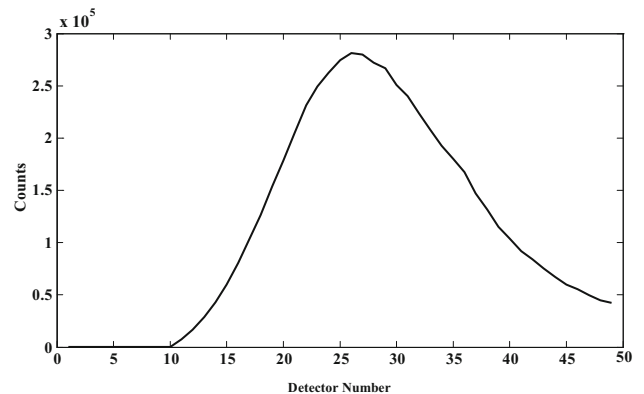


Fig. 4 Horizontal axis is each number of detectors. Vertical axis is the count of radiations passing through each detector

of each band ($d_{\varphi\alpha}$), calculated by Eq. (1); in addition, ρ and μ are arbitrary values for reinforcing these differences.

$$d_{\varphi\alpha} = \rho^* \left(\frac{D_{\varphi\alpha+1} - D_{\varphi\alpha}}{D_{\varphi\alpha+1} + D_{\varphi\alpha}} \right)^\mu \quad (1)$$

Figure 5 is the result of applying Eq. (1) on the collected counts obtained from different detectors in the first projection (at 0°). The band containing the radioactive source is clearly visible.

The counts obtained after simulation for each detector in different projections were reconstructed after being transferred to MATLAB software by the command “iradon,” based on the FBP technique; the final image is illustrated in Fig. 6. An imaginary point source was also placed within a uniform matrix through using MATLAB software, and then 60 projections were provided by the command “radon.” Then, the mentioned point was reconstructed by the command “iradon” (Fig. 6a). Figure 6 shows that the point image emerged as plus (+) after reconstruction from its projections due to the limitation of the command “iradon” in MATLAB software. This software uses the back projection method for image reconstruction based on projections; the main problem with this method is the star artifact that is shown in Fig. 6a. All photons received by the detectors have energy of 140 keV due to the lack of scattering in the environment. Thus, spectrum evaluation of detected photons’ energy was not possible and deemed meaningless.

Sensitivity is defined as the number of counts passing through the detectors per second per megabecquerel of source (cps/MBq). Geometric sensitivity of ROD in each projection was different with respect to other projections, because radioactive source position varied in the face of ROD in each projection. Mean, maximum, and minimum sensitivity in 60 projections are presented in Table 1. Sensitivity was calculated before and after subtracting two consecutive detectors by Eq. (1).

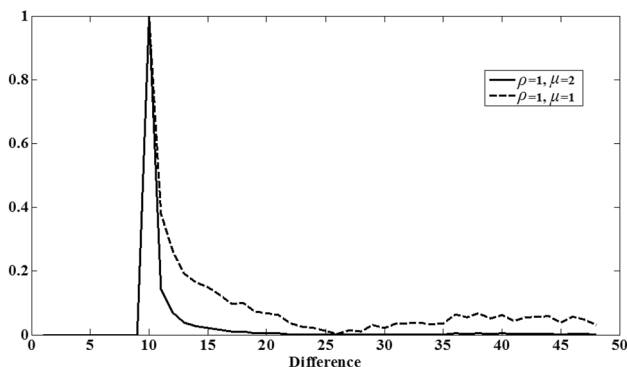


Fig. 5 Subtracting two consecutive detectors based on Eq. (1) in first projection (angle of 0°). The band containing radioactive source is clearly visible

4 Discussion

Sixty simulations were conducted by rotation of detectors around the radioactive point in 60 projections using MCNP-4C code; then data were transferred, differences were counted with Eq. (1) by MATLAB software, and the space was threaded in each projection. Figure 6b shows the outcome of this action. The star pattern around the point source results from the image reconstruction process [22], as a sharp curve appeared after subtracting (Fig. 5), and the band containing radioactive source was clearly visible. Proving this issue, a zero matrix was built in order to determine the contribution of blurring the image in running the command “iradon” in MATLAB software for the image reconstruction process. Digit 1 was placed as one of its elements, similar to radioactive source, in front of the detectors. After that, ideal projections were made by the command “radon” and the point’s image was reconstructed by the command “iradon.” Figure 6a shows the outcome of this action. The comparison made between this image and the reconstructed image through 60 projections in MCNP-4C code (Figs. 6b, c) indicates that lack of clarity in the image is related to running the command “iradon.” As a result of the comparison made between point T, resulting from the simulation with point + due to the command “radon,” the hypothesis of the elimination of collimators through detectors’ zigzag distribution ideally is verified, even though the radioactivity in the reconstructed images can be achieved without shadow by edge filters (e.g., Roberts filter). Regarding the study’s aim (investigating the possibility of omitting collimator and observing a radioactive source by a special distribution of detectors), the simulation of various sources at different distances from the camera or the distribution of radioactive material has not been dealt with and will be a future research topic. MCS and practical construction of slit–slat collimators have been investigated for resolution and sensitivity along the axis and perpendicular to the axis as a function of aperture [23, 24]. Saad et al. [25] also used MCS to find the best mesh in PHC for breast imaging. Islamian et al. [26] have applied MCS to investigate the suitable thickness of collimators.

Since the real structure of the detector was not considered in the simulations, the crossing of each photon from the small plate—considered a detector—was recorded, and the beam was assumed to have been completely absorbed. Therefore, the scattering due to photons’ interaction with the detector components was not taken into account; instead, it was assumed that each beam crossing from the detector surface was recorded by the detector, put aside, and could not penetrate adjacent detectors. In fact, penetration of beam to adjacent detectors occurs and should be

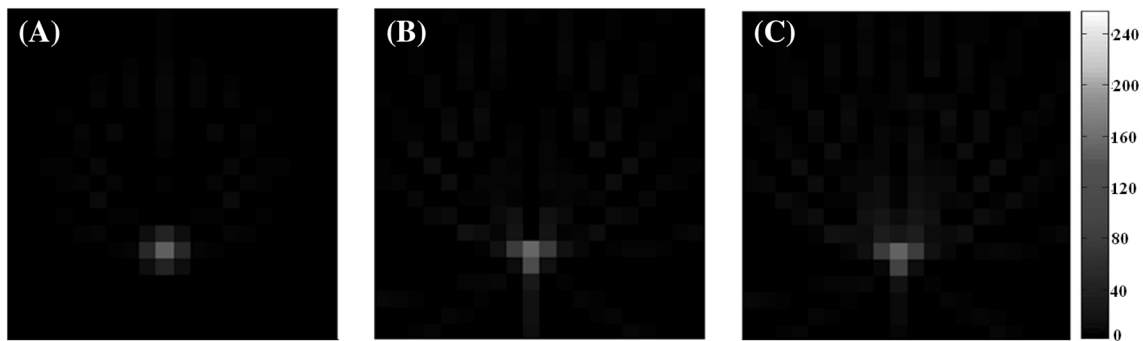


Fig. 6 **a** The reconstructed image made from 60 projections produced from an ideal point using MATLAB software's "radon" command. **b** Image reconstruction by 60 simulated projections using

MCNP-4C code with normalization values $\mu = 2$ and $\rho = 1$. **c** Image reconstruction of 60 simulated projections using code MCNP-4C with normalization values $\mu = 1$ and $\rho = 1$

Table 1 Row of detectors of sensitivity of gamma camera without collimator (GCWC), using 10^8 photons that were released from the radioactive source and were traced by Monte Carlo simulation

(MCS), totaling 60 projections presented before and after subtracting two consecutive detectors

	Mean \pm SD (cps/MBq)	Max (cps/MBq)	Min (cps/MBq)
Before subtraction	$(4.1 \pm 0.72) \times 10^3$	5.4×10^3	3.3×10^3
After subtraction	$29.5.6 \pm 96.3$	540	203.8

SD standard deviation

considered. Penetration and scattered photons in the collimator have a major impact on nuclear medicine imaging [27–29].

The goal behind using collimators is to thread the space in each projection and to determine the bands including radioactive points, and then to obtain the distribution of radioactive material through intersection of stripped spaces by different projections.

The main problem in using collimators is that most of the radiation containing information is eliminated for threading. However, in the above-mentioned method, the detectors receive the majority of information-containing radiations. As a result, the sensitivity of GCWC (Table 1) is higher than of PHC and PCs [30–32]. Therefore, according to Eq. (1), through the difference between the two detectors' data, a string can be created that can be seen by one detector and not by the other detectors (Fig. 2).

Apparently there is no difference between the presence of collimators or the above-mentioned method, and sensitivity after subtracting (Table 1) is approximately similar to conventional gamma camera [16, 17]. For example, sensitivity was obtained with 10 cameras used for Tc-99m thyroid scintigraphy by Seret et al. [31]. Measured minimum–maximum values of sensitivity were 62–131 cps/MBq for six pinhole cameras and 55–85 cps/MBq for four non-pinhole cameras. Additionally, Fleming et al. [32] reported sensitivity of two kinds of SPECT, using ^{99m}Tc at 120.2 and 153 cps/MBq. Nevertheless, it is worth

mentioning that the strings made up of two adjacent detectors produce the maximum spatial resolution. The image quality can be improved by making strings at the distance of two detectors or more; besides, it is possible to correct the final image through combining several images with various strings' widths.

When two adjacent detectors observe the radioactive material clearly, the counts of these two detectors will rise. Therefore, their difference may be much greater than the difference between two border detectors (one discerns radioactive source but the other does not) with just a few counts. Each difference will be divided by the sum of counts of two detectors in order to reinforce the difference between the two small values relative to that of the two large values. The point will be observed vividly in this stage, although it is possible to affect border reinforcement or final image clarification by changing the coefficient or power in Eq. (1). For example, in Fig. 6, the effect of selecting ($\rho = 1$, $\mu = 2$) is noted compared with ($\rho = 1$, $\mu = 1$).

Clearly, if several RODs are separated by septa, detectors will be distributed in two dimensions (Fig. 1). Therefore, a volumetric image will be formed instead of a sectional one when the camera rotates around the patient. If two parallel heads are used instead of a one-head system, increasing image-making potential, the applied corrections, and imaging speed during recording will be observed. As a result, some corrections can be imagined for GCWC,

which could inspire future research. The topics could well include optimizing the number and size of detectors, suitable angle of detectors, taking account of the corrections due to the influence of the radiations from adjacent detectors, and absorption of scattered radiations.

5 Conclusion

Simulation of gamma camera with arrangement of zig-zag detectors using MCNP-4C code in 60 projections has revealed that the space can be threaded and the radioactive source can be determined through image reconstruction without using collimator, and can instead be accomplished through a special distribution of the detectors. Simulation was conducted ideally to prove the main idea; issues, such as scattering of beam due to striking detector components, the beam passing through a detector and recording in another detector, are related to photons' collision with the material in a real location, which can affect image quality and have not been considered in the simulation. These issues should be taken into account for simulation of real GCWC in the future.

Acknowledgments The authors would like to thank S. Skies and S. A. Sabbagh for editing this manuscript.

References

- M.N. Wernick, J.N. Aarsvold, *Emission Tomography: The Fundamentals of PET and SPECT* (Elsevier Academic Press, Amsterdam, 2004), pp. 65–75
- R.A. Powsner, E.R. Powsner, *Essential Nuclear Medicine Physics* (Blackwell Pub, Malden, 2006), pp. 16–17
- C. Robert, G. Montémont, V. Rebuffel et al., Optimization of a parallel hole collimator/CdZnTe gamma-camera architecture for scintimammography. *Med. Phys.* **38**, 1806–1819 (2011). doi:10.1118/1.3560423
- R.J. Jaszczak, K.L. Greer, R.E. Coleman, SPECT using a specially designed cone beam collimator. *J. Nucl. Med.* **29**, 1398–1405 (1988)
- B.M.W. Tsui, G.T. Gullberg, E.R. Edgerton, Design and clinical utility of a fan beam collimator for SPECT imaging of the head. *J. Nucl. Med.* **27**, 810–819 (1986)
- S.P. Mueller, J.F. Polak, M.F. Kijewski et al., Collimator selection for SPECT brain imaging: the advantage of high resolution. *J. Nucl. Med.* **27**, 1729–1738 (1986)
- B. Sivertsen, S. Omvik, S. Pallesen et al., Cognitive behavioral therapy vs zopiclone for treatment of chronic primary insomnia in older adults: a randomized controlled trial. *JAMA* **295**, 2851–2858 (2006). doi:10.1001/jama.295.24.2851
- J.P. Soeffing, K.L. Lichstein, S.D. Nau et al., Psychological treatment of insomnia in hypnotic-dependant older adults. *Sleep Med.* **9**, 165–171 (2008). doi:10.1016/j.sleep.2007.02.009
- P. Paredes, S. Vidal-Sicart, G. Zanón et al., Radioguided occult lesion localisation in breast cancer using an intraoperative portable gamma camera: first results. *Eur. J. Nucl. Med. Mol. Imaging* **35**, 230–235 (2008). doi:10.1007/s00259-007-0640-x
- M.A. Ghanem, A.H. Elgazzar, M.M. Elsaid et al., Comparison of pinhole and high-resolution parallel-hole imaging for nodular thyroid disease. *Clin. Nucl. Med.* **36**, 770–771 (2011). doi:10.1097/RLU.0b013e318219ac29
- W. Branderhorst, B. Vastenhouw, F. Van Der Have et al., Targeted multi-pinhole SPECT. *Eur. J. Nucl. Med. Mol. Imaging* **38**, 552–561 (2011)
- Q.S. Dai, Channel model of pinhole gamma camera. *Chin. Sci. Bull.* **56**, 2758–2763 (2011). doi:10.1007/s11434-011-4606-9
- J. Mejia, O.Y. Galvis-Alonso, A.A. de Castro, A clinical gamma camera-based pinhole collimated system for high resolution small animal SPECT imaging. *Braz. J. Med. Biol. Res.* **43**, 1160–1166 (2010). doi:10.1590/S0100-879X2010007500128
- F.P. DiFilippo, Geometric characterization of multi-axis multi-pinhole SPECT. *Med. Phys.* **35**, 181–194 (2008). doi:10.1118/1.2821703
- S. Shokouhi, S.D. Metzler, D. Wilson et al., Multi-pinhole collimator design for small-object imaging with SiliSPECT: a high-resolution SPECT. *Phys. Med. Biol.* **54**, 207–225 (2009). doi:10.1088/0031-9155/54/2/003
- C. Vanhove, M. Defrise, T. Lahoutte et al., Three-pinhole collimator to improve axial spatial resolution and sensitivity in pinhole SPECT. *Eur. J. Nucl. Med. Mol. Imaging* **35**, 407–415 (2008). doi:10.1007/s00259-007-0579-y
- M. Rasouli, A. Takavar, M.R. Ay et al., Effects of crystal pixel size and collimator geometry on the performance of a pixelated crystal γ -camera using Monte Carlo simulation. *J. Nucl. Med. Technol.* **38**, 199–204 (2010). doi:10.2967/jnmt.109.073072
- I. Buvat, S. Laffont, J. Le Cloirec et al., Importance of the choice of the collimator for the detection of small lesions in scintimammography: a phantom study. *Phys. Med. Biol.* **46**, 1343–1355 (2001). doi:10.1088/0031-9155/46/5/301
- M.N. Wernick, J.N. Aarsvold, *Emission Tomography: The Fundamentals of PET and SPECT* (Elsevier Academic Press, Amsterdam, 2004), pp. 153–163
- M. Rafecas, G. Boning, B.J. Pichler et al., Inter-crystal scatter in a dual layer, high resolution LSO-APD positron emission tomograph. *Phys. Med. Biol.* **48**, 821–848 (2003)
- International Atomic Energy A, *Technetium-99m Radiopharmaceuticals: Manufacture of Kits* (International Atomic Energy Agency, Vienna, 2008), pp. 1–9
- J.T. Bushberg, *The Essential Physics of Medical Imaging* (Lippincott Williams & Wilkins, Philadelphia, 2002), pp. 37–373
- S.D. Metzler, R. Accorsi, J.R. Novak et al., On-axis sensitivity and resolution of a slit-slat collimator. *J. Nucl. Med.* **47**, 1884–1890 (2006)
- A. Kamali-Asl, S. Sarkar, M. Shahriari et al., Slit slat collimator optimization with respect to MTF. *Appl. Radiat. Isot.* **62**, 461–468 (2005). doi:10.1016/j.apradiso.2004.07.009
- W.H.M. Saad, R.E. Roslan, M.A. Mahdi et al., Monte Carlo design of optimal wire mesh collimator for breast tumor imaging process. *Nucl. Instr. Meth. Phys. Res. A* **648**, 254–260 (2011). doi:10.1016/j.nima.2011.05.064
- J.P. Islamian, M.T. Toossi, M. Momenzad et al., Monte Carlo study of the effect of collimator thickness on T-99m source response in single photon emission computed tomography. *World J. Nucl. Med.* **11**, 70–74 (2012). doi:10.4103/1450-1147.103419
- D. Autret, A. Bitar, L. Ferrer et al., Monte Carlo modeling of gamma cameras for I-131 imaging in targeted radiotherapy. *Cancer Biother. Radiopharm.* **20**, 77–84 (2005). doi:10.1089/cbr.2005.20.77
- A. Larsson, M. Ljungberg, S.J. Mo et al., Correction for scatter and septal penetration using convolution subtraction methods and model-based compensation in ^{123}I brain SPECT imaging—a Monte Carlo study. *Phys. Med. Biol.* **51**, 5753–5767 (2006). doi:10.1088/0031-9155/51/22/003

29. M.F. Smith, R.J. Jaszczak, The effect of gamma ray penetration on angle-dependent sensitivity for pinhole collimation in nuclear medicine. *Med. Phys.* **24**, 1701–1709 (1997)
30. F. Beekman, F. van der Have, The pinhole: gateway to ultra-high-resolution three-dimensional radionuclide imaging. *Eur. J. Nucl. Med. Mol. Imaging* **34**, 151–161 (2007). doi:[10.1007/s00259-006-0248-6](https://doi.org/10.1007/s00259-006-0248-6)
31. A.A. Seret, A comparison of contrast and sensitivity in Tc-99m thyroid scintigraphy between nine nuclear medicine centres of a geographic area. *Alasbimn J.* **32**, 32–33 (2006)
32. J.S. Fleming, A.S. Alaamer, Influence of collimator characteristics on quantification in SPECT. *J. Nucl. Med.* **37**, 1832–1836 (1996)